Propellants,
Explosives,
Pyrotechnics

DOI: 10.1002/prep.201500313

Study on the Viscoelastic Poisson's Ratio of Solid Propellants Using Digital Image Correlation Method

Hui Ru Cui,[a] **Guo Jin Tang,**[a] **and Zhi Bin Shen***[a]

Abstract: Digital image correlation methods were used for further studies of the viscoelastic Poisson's ratio of solid propellants. The Poisson's ratio and the Young's relaxation modulus of solid propellants were separately determined in a single stress relaxation test. In addition, the effects of temperature, longitudinal strain, preload and storage time on the Poisson's ratio of solid propellants were discussed. The Poisson's ratio master curve and the Young's relaxation modulus master curve were constructed based on the time-temperature equivalence principle. The obtained results showed that the Poisson's ratio of solid propellants is a monotone non-decreasing function of time, the instantaneous Poisson's ratio increased from 0.3899 to 0.4858 and the time of the equilibrium Poisson's ratio occurred late when the temperature was varied from −30 °C to 70 °C. The Poisson's ratio increased with temperature and longitudinal strain, decreased with preload and storage time, while the amplitude Poisson's ratio increased with preload, decreases with longitudinal strain and storage time. The time of the equilibrium Poisson's ratio occurred in advance with the increase of longitudinal strain, preload and storage time.

Keywords: Solid propellants · Viscoelastic Poisson's ratio · Longitudinal strain · Preload · Storage time

---

1 Introduction

The viscoelastic Poisson's ratio, $\nu(t)$, is a material mechanical property, which is closely related to time, temperature, and strain [1–11]. Solid propellants are viscoelastic materials and the Poisson's ratio of solid propellants is an essential input parameter in structural integrity analysis of solid rocket motors (SRM). It has been shown that changes of the Poisson's ratio in micrometer level have great influence on the structural integrity analysis of solid rocket motors [12,13]. It is commonly assumed that the Poisson's ratio is a material constant and independent of temperature and strain [14,15]. In addition, the aging effect on the Poisson's ratio attracts attention in the shelf life prediction of propellants [16]. Thus, there are practical as well as theoretical aspects that make it highly desirable to stimulate the experimental determination of the Poisson's ratio of solid propellants on a secure analytical foundation.

Previously, it has been attempted to use many direct or indirect methods measure viscoelastic Poisson's ratio for a long time. Kugler et al. measured both the uniaxial extension and the lateral contraction on a glass bead filled, compounded Hypalon rubber using electro-optical extensometer in stress relaxation tests. They conducted the stress relaxation tests at five constant strain levels and accounted for the strain-dependence of the Poisson's ratio through an equation of Smith [17,18]. Knauss et al. measured the time-dependent Poisson's ratio of commercial poly by using a speckle interferometric technique at 12 temperatures ranging from 25 °C to 125 °C [19]. Chen et al. used dynamic thermomechanical analysis (DMA) to simultaneously acquire Young's relaxation modulus and time-dependent Poisson's ratio of an epoxy molding compound (EMC) with the assumption of constant bulk modulus. They found the viscoelastic Poisson's ratio of EMC varies significantly over time from 0.4 to 0.496, and can't be assumed as a constant [8]. Md et al. conducted relaxation tests at different temperatures in diametrical mode to obtain Poisson's ratio of asphalt concrete (AC) [7]. In addition, they also performed cyclic load test at different temperatures and loading frequencies to determine the temperature- and frequency-dependent Poisson's ratio of AC. Measurements of viscoelastic moduli in torsion and bending have been conducted at ambient temperature, 22 °C, using broadband viscoelastic spectroscopy by Dong. The Poisson's ratio was inferred from frequency-dependent torsional and bending moduli [9].

Based on the integral transform relations of stress relaxation modulus, body modulus and viscoelastic Poisson's ratio, the viscoelastic Poisson's ratio of solid propellants was calculated by using the inversion of Laplace transform and numerical integral [1]. He et al. built cylindrical motors method to determine the Poisson's ratio of solid propellants [5]. According to the maximum radial deformations of the perforations of cylindrical motors with two different outer-inner radial ratios after having been cured and drop-

---

[a] *H. R. Cui, G. J. Tang, Z. B. Shen*
College of Aerospace Science and Engineering
National University of Defense Technology
Changsha 410073, P. R. China
**e-mail: 15651710682@163.com*

ped in the temperatures, the Poisson's ratio at different temperatures was fit out by use of FEM.

Experimental determination of the time-dependent viscoelastic Poisson's ratio of solid propellants using an accuracy-enhanced 2D digital image correlation method (DICM) has been conducted by Pan [10,20–24]. The results reveal that, by adequately eliminating the measurement errors associated with the unavoidable out-of-plane displacements and lens distortion, the present DICM can be used for precise determination of the viscoelastic Poisson's ratio of solid propellants. The successful, highly accurate, simultaneous determination of two viscoelastic response functions is of great theoretical interest. However, the Young's relaxation modulus was not determined in his test and the effects of temperature, longitudinal strain, preload, and storage time was not considered in his study. In addition, the Poisson's ratio is so high and shows an increasing trend to the incompressible value of 0.5 within 1000 s at ambient temperature. Therefore, further studies are needed to analysis the effects of temperature, longitudinal strains, preload, and storage time on the Poisson's ratio of solid propellants using DICM.

From the above discussion, it is evident that the Poisson's ratio and the Young's relaxation modulus of solid propellants have not been determined in a single test separately, so far, through stress relaxation test. The Poisson's ratio master curve simultaneous to the Young's relaxation modulus master curve of solid propellants based on the time-temperature equivalence principle which is required for the structural integrity analysis of SRM in time domain, the effects of temperature, longitudinal strain, preload and storage time on Poisson's ratio of solid propellants are studied herein.

2 Objectives

The main objectives of the study are to:

(a) Determine the time and temperature dependent Poisson's ratio of solid propellants using DICM simultaneously acquires the Young's relaxation modulus by stress relaxation test.
(b) Construct the Poisson's ratio master curve and Young's relaxation modulus master curve based on the time-temperature equivalence principle.
(c) Analyze the factors, which affect the value of Poisson's ratio, including longitudinal strain, preload and storage time.

3 Principles of Measurement

3.1 Digital Image Correlation Method

DICM is a technology that using computer to process images through a certain algorithm. DICM uses CCD (charge-coupled device) camera to record the digital speckle patterns of tested surface before and after deformation. The sub-region around each point on the speckle filed may show distinctly different intensity distribution characteristics which will help DICM measure displacement and deformation of the point by using some search algorithm.

Figure 1(a) shows the speckle pattern before deformation and *I*(*x*, *y*) is used to characterize it's grey field. Figure 1(b) is the speckle pattern after deformation and *I*′(*x*′, *y*′) is used to characterize it's grey field. *P*(*x*, *y*) is a point on tested surface and a sub-region A centered around the point is selected sized at $m \times n$ pixels. Sub-region A will move to a new position and change its shape, the new region is called sub-region A′, simultaneously the grey field changes from *I*(*x*, *y*) to *I*′(*x*′, *y*′) and the central point of sub-region A changes from *P*(*x*, *y*) to *P*′(*x*′, *y*′). By this stage, the grey field of sub-region A and sub-region A′ will get the maximal correlation coefficients.

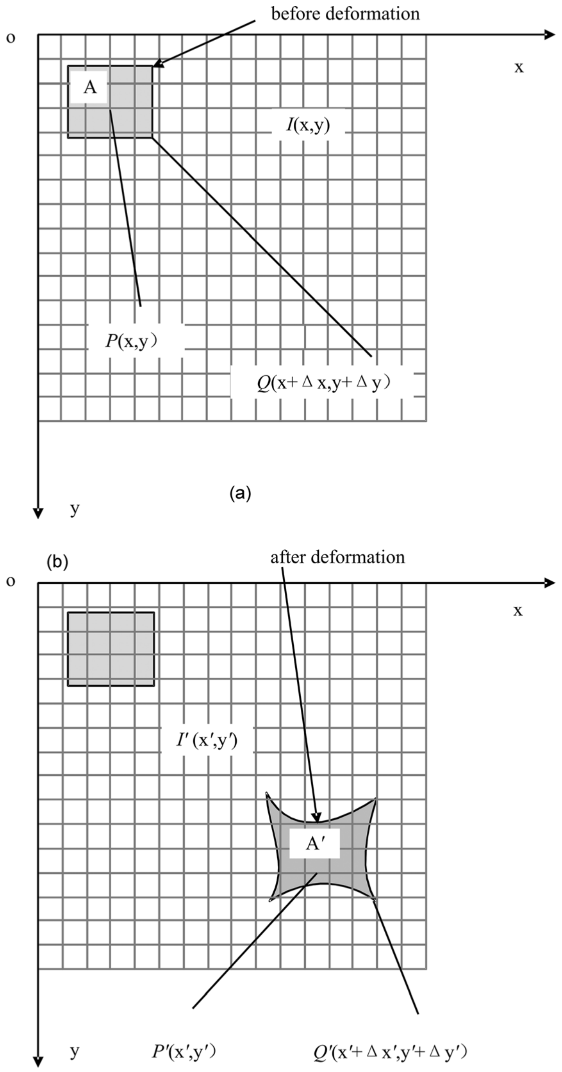

Figure 1. Schematic diagram of DICM.

By using a certain algorithm to make correlation operation, the sub-region A′ centered around the point $P'(x', y')$ will be found after deformation when the grey field of sub-region A and Sub-region A′ get the maximal correlation coefficients. The displacement components of $P'(x', y')$, $u(x, y)$ and $v(x, y)$, can be expressed as [23,24]:

$$\begin{cases} u(x,y)=x'-x \\ v(x,y)=y'-y \end{cases} \tag{1}$$

The full displacement field can be obtained after dealing with enough points of the speckle pattern follow the instructions above. Figure 2(a) and Figure 2(b) are a set of results, from which we can get the displacement in the x and y direction.

In order to obtain full strain field, the continuous displacement field is measured based on least-square fitting first. The displacement can be predicted by displacement polynomial function. For example, the x and y directional virtual displacements can be expressed as:

$$\begin{cases} u(x,y)=a_0+a_1x+a_2y \\ v(x,y)=b_0+b_1x+b_2y \end{cases} \tag{2}$$

where a_0, a_1, a_2, b_0, b_1, and b_2 are parameters.

Full strain field will be obtained with the displacement polynomial function above based on the geometric relationship between the displacement and strain. For the condition of small deformation, the Cauchy strain can be expressed as

$$\begin{cases} \varepsilon_x=\dfrac{\partial u(x,y)}{\partial x}=a_1 \\ \varepsilon_y=\dfrac{\partial v(x,y)}{\partial y}=b_2 \\ \gamma_{xy}=\dfrac{\partial u(x,y)}{\partial y}+\dfrac{\partial v(x,y)}{\partial x}=a_2+b_1 \end{cases} \tag{3}$$

or, for the condition of limited deformation, the Green strain can be expressed as:

$$\begin{cases} \varepsilon_x=\dfrac{\partial u}{\partial x}+\dfrac{1}{2}[(\dfrac{\partial u}{\partial x})^2+(\dfrac{\partial v}{\partial y})^2]=a_1+\dfrac{1}{2}(a_1^2+b_1^2) \\ \varepsilon_y=\dfrac{\partial v}{\partial y}+\dfrac{1}{2}[(\dfrac{\partial u}{\partial y})^2+(\dfrac{\partial v}{\partial y})^2]=b_2+\dfrac{1}{2}(a_2^2+b_2^2) \\ \gamma_{xy}=\dfrac{1}{2}(\dfrac{\partial u}{\partial y}+\dfrac{\partial v}{\partial x})+\dfrac{1}{2}(\dfrac{\partial^2 u}{\partial x\partial y}+\dfrac{\partial^2 v}{\partial x\partial y}) \\ \quad =\dfrac{1}{2}(a_2+b_1)+\dfrac{1}{2}(a_1a_2+b_1b_2) \end{cases} \tag{4}$$

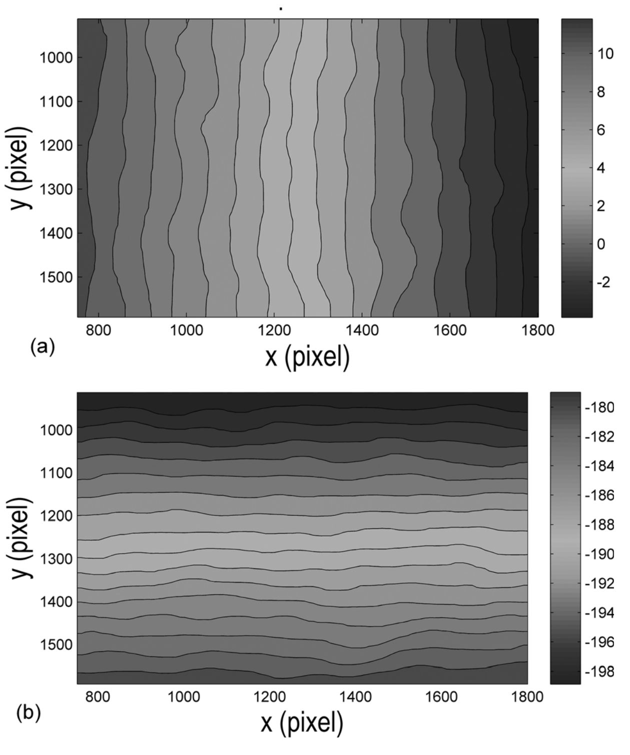

Figure 2. Displacement distribution of x and y direction (a) x displacement, (b) y displacement.

3.2 Viscoelastic Poisson's Ratio

The viscoelastic Poisson's ratio, $\nu(t)$, is defined as resulting from the response of a homogeneous isotropic material to the imposition of a step function of time, $h(t)$, in the infinitesimal uniaxial extension. Given that the deformation is a strain, ε_x^0, applied in the x direction, the viscoelastic Poisson's ratio can be expressed as [11]:

$$\nu(t)=-\varepsilon_y(t)/\varepsilon_x^0 \tag{5}$$

where ε_x^0 is the longitudinal deformation in the x-direction, whereas $\varepsilon_y(t)$ is the deformation in one of the transverse directions.

The viscoelastic Poisson's ratio, $\nu(t)$, can be obtained by stress relaxation test based on the definition above. The longitudinal deformation is always relative to the time for the laboratory apparatus can't provide step longitudinal deformation actually. The total response of the system can be regarded as linear superposition of numerous tiny responses based on the Boltzmann overlapping principle through dividing the time into a series of time intervals. If the tiny step longitudinal deformation is $d\varepsilon_x(\tau)$ for time τ, the lateral strain is $d\varepsilon_y(t)=-\nu(t-\tau)\, d\varepsilon_x(\tau)$ for time t, which varies continuously within the range of $[0, t]$. The total lateral strain can be obtained based on the Boltzmann overlapping principle and expressed as [1]:

$$\varepsilon_y(t)=-\int_{-\infty}^{t}\nu(t-\tau)\frac{\partial\varepsilon_x(\tau)}{\partial\tau}\mathrm{d}\tau \tag{6}$$

The response of the lateral strain, $\varepsilon_y(t)$, always lags behind longitudinal strain, $\varepsilon_x(t)$, which can be predicted from Equation (6). The viscoelastic Poisson's ratio, $\nu(t)$, is a memory function of the lateral strain, $\varepsilon_y(t)$. There is a hereditary integral relationship between $\nu(t)$, $\varepsilon_y(t)$, and $\varepsilon_x(t)$

rather than a simple algebraic relation. Further, from Equation (6) it can be conlcuded:

$$-\varepsilon_y(t)=\nu(t)\varepsilon_x^0+\int_0^t \nu(t-\tau)\frac{\partial\varepsilon_x(\tau)}{\partial\tau}\mathrm{d}\tau \tag{7}$$

If it is assumed that $\varepsilon_x(t)\simeq\varepsilon_x^0$, then Equation (7) can be simplified as:

$$\nu(t)\cong-\varepsilon_y(t)/\varepsilon_x^0 \tag{8}$$

As a supplement to introduce, the Prony series of Poisson's ratio can be expressed as:

$$\nu(t)=\nu_0+\sum_{n=1}^{N_\nu}\nu_n(1-e^{-\frac{t}{\tau_n^\nu}}) \tag{9}$$

or, equivalently:

$$\nu(t)=\nu_\infty-\sum_{n=1}^{N_\nu}\nu_n e^{-\frac{t}{\tau_n^\nu}} \tag{10}$$

where ν_0 is the instantaneous Poisson's ratio, ν_∞ is the equilibrium Poisson's ratio, N_ν is the number of terms in the Prony series, t represents time, τ_n^ν and ν_n are undetermined coefficients. In addition, this paper introduces the time for reaching the equilibrium Poisson's ratio, t_E, and the amplitude Poisson's ratio which can be expressed as:

$$\nu_A=\nu_\infty-\nu_0 \tag{11}$$

4 Laboratory Test

4.1 Specimen, Fixture, and Test System

The material studied in this paper is hydroxyl-terminated poly-butadiene (HTPB) propellant. The test tensile specimen is designed as a dumbbell-salt shape according to the aerospace industry standard of PRC, QJ 924–85, as shown in Figure 3(a). A fixture is designed, as illustrated in Figure 3(b), used to hold the test tensile specimen and keep the uniaxial extension.

The test system includes two parts, image collecting subsystem and test environment subsystem, as illustrated in Figure 4 and Figure 5. Light source is used to avoid the influence of nature light and provide a brighter vision in test chamber. We use the bilateral telecentric lens and a 5.1 megapixel CCD camera to record real-time digital speckle patterns when the test runs. The centerline of the lens is still prependicular to the surface of specimen. The storage and caculation of the images are processed by computer automatically. The image collecting subsystem can get a clear image of the sample surface with a field of view of 5×5 mm^2.

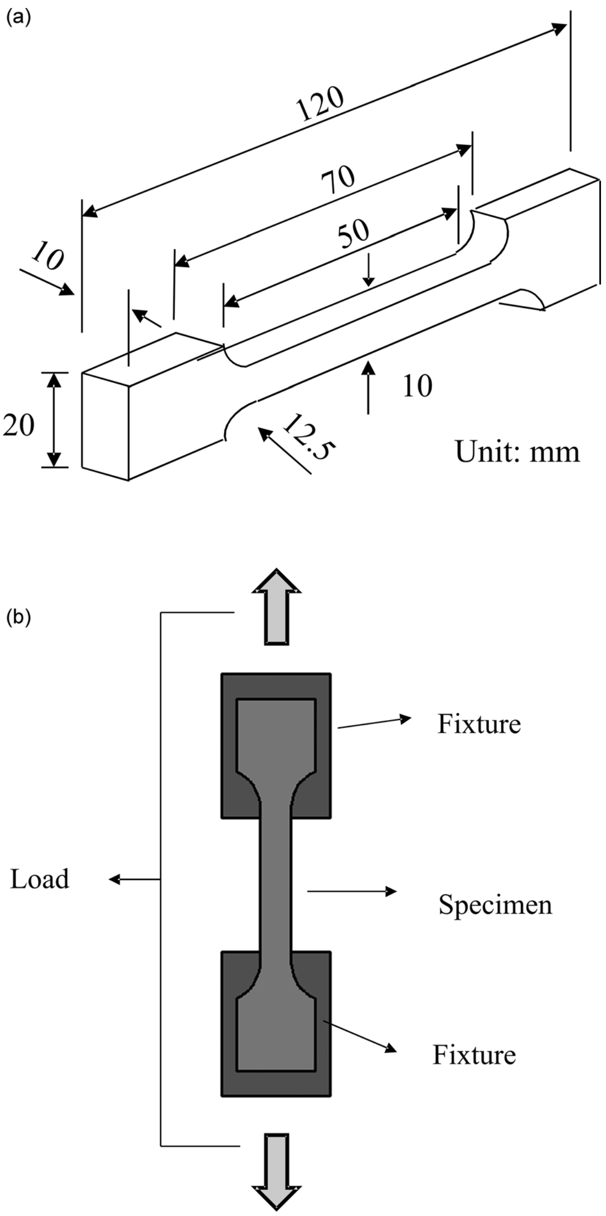

Figure 3. Test specimen and it's fixture.

The test under low temperature required for the properities of SRM at low temperature is strongly concerned. The test environment subsystem can provide different temperature conditions with the heating and cooling unit. The hot and cold stream are transmitted to test chamber through pipe unit. Two thick screw rods connect the fixtures with upper beam and movable beam in order to good alignment capability and stable retaining the specimen. The maximal speed of the movable beam can reach to 600 mm min^{-1}. The force sensor records the force on the specimen from which we can get the Young's relaxation modulus.

The test window, as illustrated in Figure 6, is special for its complex constructs and purpose. The transparency of the test window is over 96%, and the complex constructs can prevent the frosting and fogging of the glass of the

DOI: 10.1002/prep.201500313

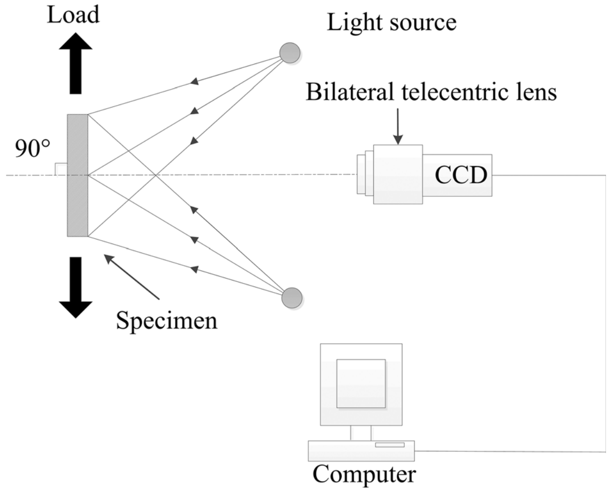

Figure 4. Image collecting subsystem.

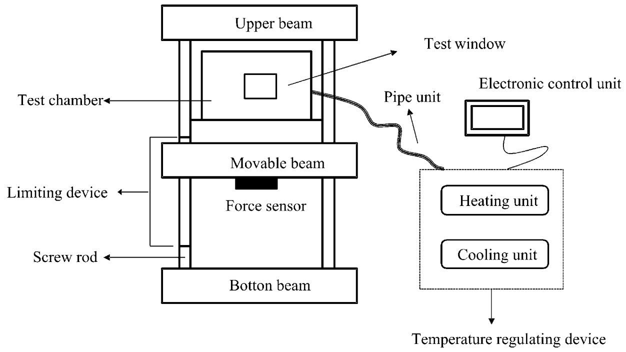

Figure 5. Test environment subsystem.

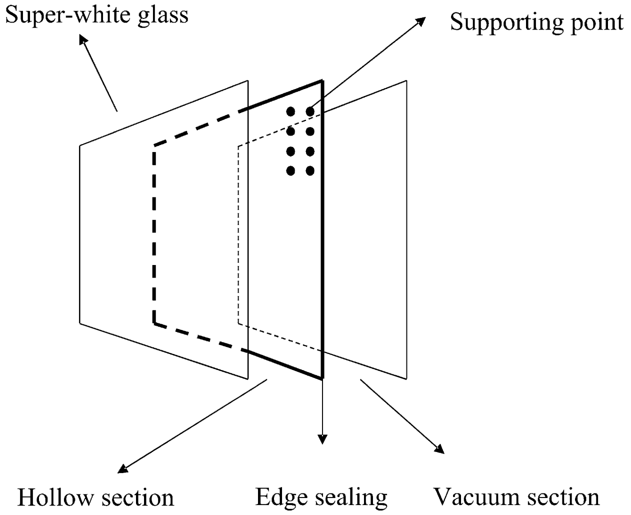

Figure 6. Schematic diagram of test window.

test window even at −30 °C. The test window is divided into two parts, hollow section and vacuum section, by three super-white glasses. The test window is sealed by edge sealing at four edges. The heat transfer coefficient of the test window can as low as 1.1 w per (m^2k) through test. The glasses won't get squashed by atmospheric pressure because of the supportive power from supporting points.

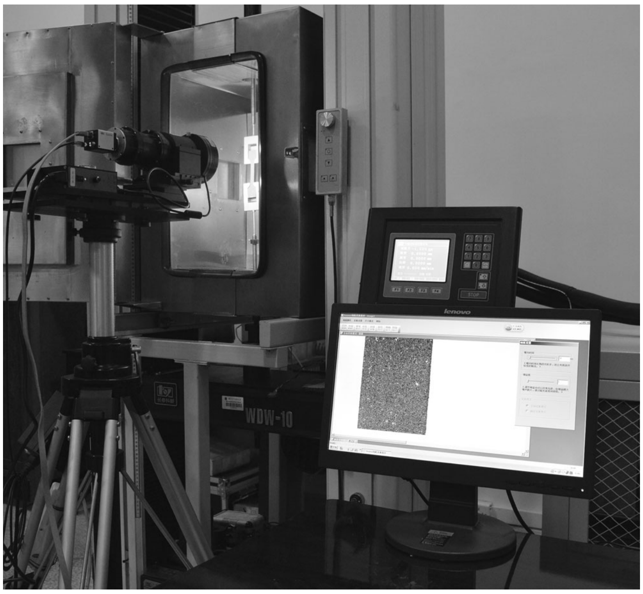

Figure 7. Image of testing scenarios.

An image of testing scenarios is shown in Figure 7, the door of the test chamber is open for clarity and it will be closed while the test runs. The digital speckle patterns of tested surface and the force recorded by the force sensor on the specimen are transmitted to the computer for further calculation.

It is worth mentioning that, in order to avoid the influence of the additional stiffness on specimen, we use the grains of aluminum on the surface of specimen as the natural speckle pattern rather than use artificial speckle which may produce errors more or less. The natural speckle pattern on the surface of specimen is shown in Figure 8.

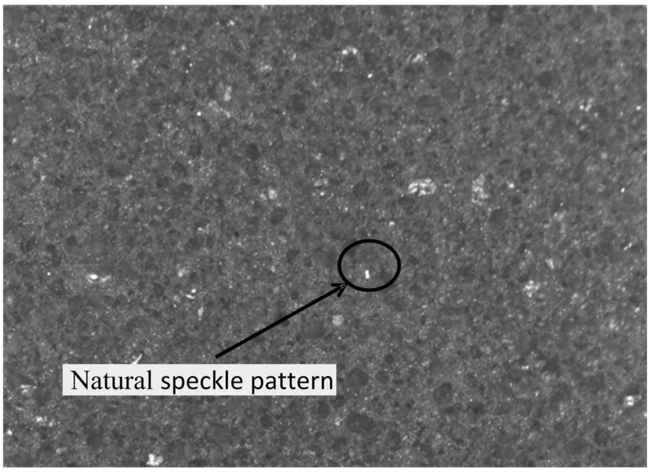

Figure 8. Natural speckle pattern on the surface of specimen.

4.2 Design of Tests

Propellants used in tests have the same components, manufactured by the same processing technique and stored in the same environment. There are 13 tests are designed to complete the objectives of this paper. The test temperatures selected covers a wide range to examine the effect of temperature on Poisson's ratio. However, the longitudinal strain selected a small range to keep the strain in the linear viscoelastic range [7]. Detailed descriptions of the tests are presented in Table 1. Note that the specimen should be under the constant test temperature for 40 min in order to achieve a completely uniform temperature distribution in the specimen body before test.

Table 1. Design of test.

No	Temperature [°C]	Longitudinal strain [%]	Preload [N]	Storage time [year]	Test time [s]
1	70	3.5	0.5	1	45000
2	50	3.5	0.5	1	45000
3	20	3.5	0.5	1	45000
4	0	3.5	0.5	1	45000
5	−15	3.5	0.5	1	45000
6	−30	3.5	0.5	1	45000
7	20	3.5	0.5	2	2500
8	20	3.0	0.5	2	2500
9	20	2.5	0.5	2	2500
10	20	3.5	1.5	2	2500
11	20	3.5	2.5	2	2500
13	20	3.5	0.5	4	2500

5 Results and Discussion

5.1 The Effects of Temperature on the Poisson's Ratio

The Poisson's ratios at different temperatures are presented in Figure 9. It shows that the Poisson's ratio of solid propellants is a monotone non-decreasing function of time. With the increase of ambient temperature, the Poisson's ratio increases. For example, the instantaneous Poisson's ratio are 0.3897, 0.4001, 0.4510, 0.4680, and 0.4858 at −30 °C, −15 °C, 0 °C, 20 °C, 50 °C, and 70 °C, respectively. The instantaneous Poisson's ratio increases by 0.0001 for 10 °C increase in temperature on average.

In addition, by fitted test results, the Poisson's ratio reached to 0.4946 which is close to 0.5 at the end of the test at 70 °C, but the value is not the equilibrium Poisson's ratio. The increment of Poisson's ratio is not significant after 3×10^4 s at 50 °C and the Poisson's ratio approaches the equilibrium Poisson's ratio, 0.4774. The equilibrium Poisson's ratio appears at −30 °C, −15 °C, 0 °C and 20 °C after 4500 s, 6500 s, 8900 s, and 10000 s, respectively. The results indicate that the time of the equilibrium Poisson's ratio occurs in advance with the increase of temperature. Moreover, the test date has better stability at lower temperature, which may be caused by less molecular motion.

The solid propellant is thermorheological simple material and the material mechanical properties always satisfy the time-temperature equivalence principle. The Poisson's ratio master curve is fitted, as illustrated in Figure 10, according to the method used on Young's relaxation modulus master curve. According to the Williams-Landel-Ferry (WLF) equation [25]:

$$\log a_T = \frac{-C_1(T-T_s)}{C_2+T-T_s} \tag{12}$$

where $\log(a_T)$ is the shift factor, T is the current temperature, T_s is the reference temperature, C_1 and C_2 are material constants.

The coefficients of WLF equation, $C_1=9.1627$, $C_2=-63.3151$, obtained based on the nonlinear least square method at the reference temperature, $T_s=20\,^\circ C$. At the same time, the Young's relaxation modulus master curve is fitted, as illustrated in Figure 11, with the coefficients of WLF equation, $C_1=22.0121$, $C_2=553.0371$, at the reference temperature, $T_s=20\,^\circ C$.

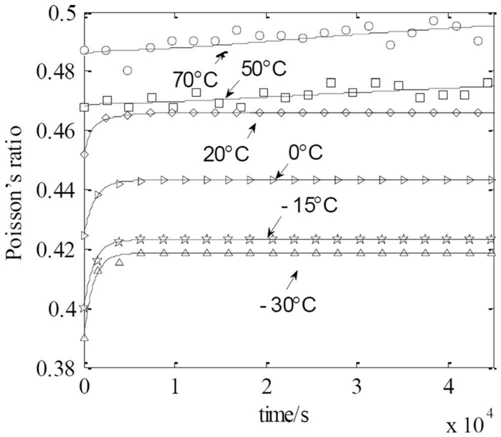

Figure 9. Result of measurement under different temperatures.

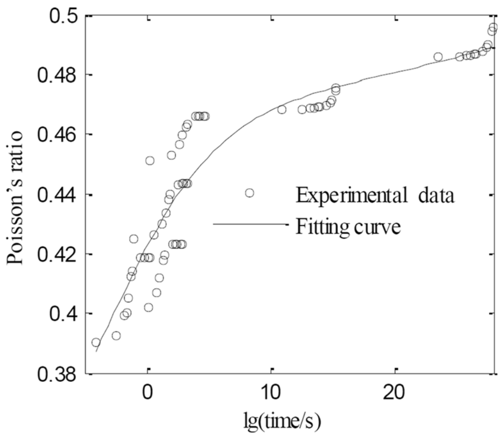

Figure 10. Poisson's ratio master curve.

DOI: 10.1002/prep.201500313

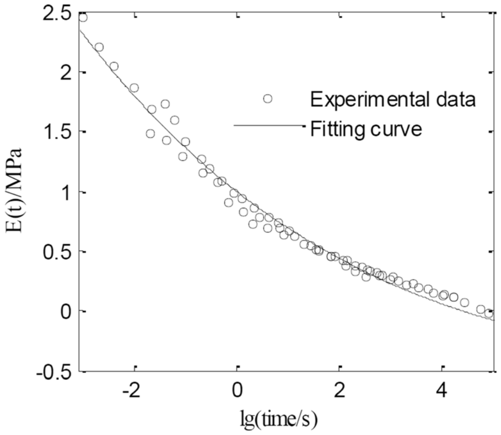

Figure 11. Young's relaxation modulus master curve.

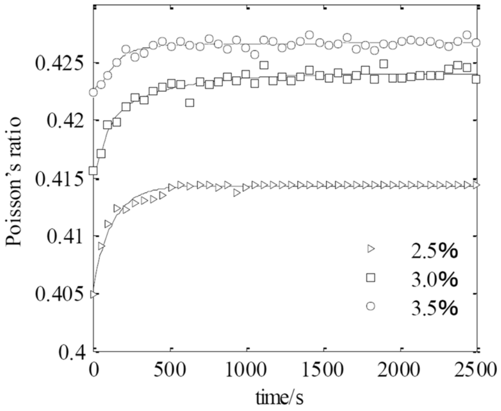

Figure 12. Result of measurement under different longitudinal strain.

5.2 Effects of Longitudinal Strain on the Poisson's Ratio

Poisson's ratios at different longitudinal strain are presented in Figure 12. It can be directly perceived through Figure 12 that the Poisson's ratio increases as the increase of longitudinal strain. The instantaneous Poisson's ratios are 0.4218, 0.4155, and 0.4053 when the longitudinal strain are 3.5 %, 3.0 %, and 2.5 %, respectively. The instantaneous Poisson's ratio increases by 0.0165 for 1 % increase in longitudinal strain on average. In addition, the amplitude Poisson's ratios are 0.0048, 0.0085 and 0.0090 when the longitudinal strain are 3.5 %, 3.0 % and 2.5 %, respectively. The amplitude Poisson's ratio decreases by 0.0042 for 1 % increase in longitudinal strain on average. Furthermore, the equilibrium Poisson's ratio occurs in advance with the increase of longitudinal strain, as we can see the time reach to the equilibrium Poisson's ratio are 500 s, 900 s, and 1000 s when the longitudinal strain are 3.5 %, 3.0 %, and 2.5 %, respectively. The parameters of the Prony series for the Poisson's ratio under different longitudinal strain are shown in Table 2, while the number of the terms in the Prony series is 5.

5.3 Effects of Preload on the Poisson's Ratio

Force is needed to hold the specimen at the beginning of the test, it may be big even the specimen is treated very carefully. The force, called preload, has important influence on stress relaxation test for the solid propellant is very sensitive to force. The Poisson's ratios at different preload are presented in Figure 13. As can be seen, the Poisson's ratio increases with the decrease of preload. For example, the equilibrium Poisson's ratios are 0.4035, 0.4193, and 0.4266 when the preload are 2.5 N, 1.5 N and 0.5 N, respectively. The equilibrium Poisson's ratio increases by 0.0111 for 1 N decrease in preload on average. It is a remarkable fact that the instantaneous Poisson's ratio can be smaller than 0.4 which is a theory deduced by Hao [2] at 20 °C. In addition, the amplitude Poisson's ratios are 0.0048, 0.0051, and 0.0063 when the preload are 0.5 N, 1.5 N and 2.5 N, respectively. The amplitude Poisson's ratio increases by 0.0040 for

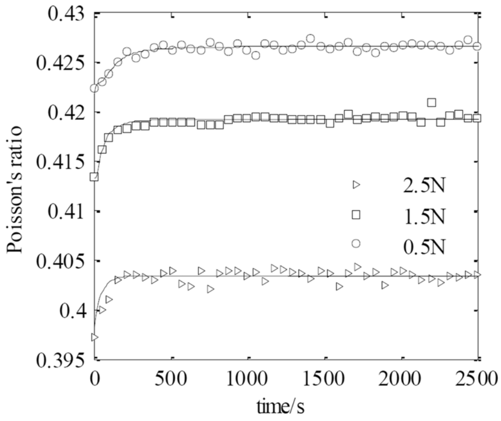

Figure 13. Result of measurement under different preloads.

Table 2. Parameters of the Prony series for the Poisson's ratio under different longitudinal strain.

Condition		$n=0$	$n=1$	$n=2$	$n=3$	$n=4$	$n=5$
$\varepsilon_x^0=2.5\,\%$	τ_n^v [s]	–	87.6985	146.4565	244.5823	408.4525	682.1157
	ν_n	0.4053	0.0087	−0.01571	0.0220	−0.0109	0.0032
$\varepsilon_x^0=3.0\,\%$	τ_n^v [s]	–	25.4806	50.9611	101.9222	203.8445	407.6889
	ν_n	0.4155	−0.0046	0.0059	0.0037	−0.0014	0.0048
$\varepsilon_x^0=3.5\,\%$	τ_n^v [s]	-	15.2631	33.5789	73.8736	162.5219	357.5483
	ν_n	0.4218	0.0040	−0.0089	0.0081	0.0011	0.0005

Table 3. Parameters of the Prony series for the Poisson's ratio under different preload.

Condition		$n=0$	$n=1$	$n=2$	$n=3$	$n=4$	$n=5$
$F=2.5$ N	τ_n^v [s]	–	1.5773	5.5205	19.3220	67.6272	236.6953
	ν_n	0.3972	0.0186	−0.0297	0.0168	−0.0018	0.0025
$F=1.5$ N	τ_n^v [s]	–	3.7317	9.7397	25.4207	66.3482	173.1689
	ν_n	0.4142	0.0097	−0.0100	0.0062	0.0046	0.0006
$F=0.5$ N	τ_n^v [s]	–	15.2631	33.5789	73.8736	162.5219	357.5483
	ν_n	0.4218	0.0040	−0.0089	0.0081	0.0011	0.0005

1 N increase in preload on average. Furthermore, the equilibrium Poisson's ratio occurs in advance with the increase of preload, as we can see the time reach to the equilibrium Poisson's ratio are 500 s, 250 s, and 150 s when the preload are 0.5 N, 1.5 N, and 2.5 N, respectively. The parameters of the Prony series for the Poisson's ratio under different preload are shown in Table 3 while the number of the terms in the Prony series is 5.

5.4 Effects of Storage Time on the Poisson's Ratio

The Poisson's ratio of propellants stored for 4 years is shown in Figure 14. The result is smaller than that obtained from propellants which stored for 1 or 2 years in Figure 11 and Figure 12 at the same test environment. As illustrated in Table 4, the instantaneous Poisson's ratio decreases from 0.4510 to 0.3955, the equilibrium Poisson's ratio decreases from 0.4664 to 0.3991, as the storage time varies from 1 year to 4 years. In addition, the amplitude Poisson's ratios are 0.0154, 0.0048, and 0.0036 when the storage times are 1 year, 2 years, and 4 years, respectively. The amplitude Poisson's ratio decreases by 0.0056 for 1 year increase in storage time on average. Furthermore, the equilibrium Poisson's ratio occurs in advance with the increase of storage time, as we can see the time reach to the equilibrium Poisson's ratio are 10000 s, 500 s and 250 s when the storage time are 1 year, 2 years and 4 years, respectively.

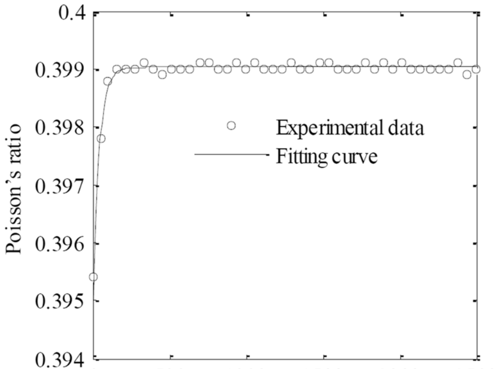

Figure 14. Poisson's ratio of propellant stored for 4 years.

Table 4. Test results of propellants with different storage time.

Storage time [year]	ν_0	ν_∞	ν_A	t_E [s]
1	0.4510	0.4664	0.0154	10000
2	0.4218	0.4266	0.0048	500
4	0.3955	0.3991	0.0036	250

6 Conclusions

The study investigates the effects of time, temperature, longitudinal strain, preload and storage time on the Poisson's ratio of solid propellants by the stress relaxation tests using DICM. The Poisson's ratio and the Young's relaxation modulus of solid propellants are determined in a single stress relaxation test separately. In addition, the Poisson's ratio master curve and the Young's relaxation modulus master curve are constructed based on the time-temperature equivalence principle. Based on the findings of the study, the following conclusions can be made

(a) The Poisson's ratio of solid propellants is a monotone non-decreasing function of time, with the increase of ambient temperature, the Poisson's ratio increases. In addition, the occurring time of the equilibrium Poisson's ratio advances with the increase of temperature. The extra high Poisson's ratio determined by Pan may be caused by the artificial speckle on the surface of the specimen; it can't represent the true state of the surface of the specimen.

(b) The Poisson's ratio master curve and Young's relaxation modulus master curve are constructed based on the time-temperature equivalence principle. The coefficients of WLF equation, $C_1=9.1627$, $C_2=-63.3151$, obtained based on the nonlinear least square method at the reference temperature, $T_s=20\,^\circ\mathrm{C}$. At the same time, the Young's relaxation modulus master curve is fitted, with the coefficients of WLF equation, $C_1=22.0121$, $C_2=553.0371$, at the same reference temperature, $20\,^\circ\mathrm{C}$.

(c) Increasing longitudinal strain, decreasing preload and storage time increase the Poisson's ratio. Decreasing longitudinal strain and storage time causes increasing preload increase the amplitude Poisson's ratio.

(d) In addition, the time of the equilibrium Poisson's ratio occurs in advance with the increase of longitudinal strain, preload and storage time.

DOI: 10.1002/prep.201500313

References

[1] B. H. Zhao, An Investigation on Viscoelastic Poisson's Ratio and Dynamic Complex Poisson's Ratio, *J. Propul. Technol.* **1995**, *3*, 1 – 7.

[2] S. L. Hao, Initial Viscoelastic Poisson's Ratio of High-filled Composite Propellant, *J. Solid Rocket Technol.* **1996**, *19*, 46 – 50.

[3] H. H. Hilton, The Elusive and Fickle Viscoelastic Poisson's Ratio and its Relation to the Elastic-Viscoelastic Correspondence Principle, *J. Mech. Mater. Struct.* **2009**, *4*, 1341 – 1364.

[4] L. Grassia, A. D. Amore, S. L. Simon, On the Viscoelastic Poisson's Ratio in Amorphous Polymers, *J. Rheology* **2010**, *54*, 1009 – 1022.

[5] T. S. He, Y. Y. Pu, Z. Q. Wang, Determining Poisson's Ratio of Solid Propellant by Means of Cylindrical Motors, *J. Propul. Technol.* **2001**, *22*, 171 – 173.

[6] R. S. Lakes, The Time-Dependent Poisson's Ratio of Viscoelastic Materials can Increase or Decrease, *Cellular Polym.* **1992**, *11*, 466 – 469.

[7] R. I. Md, M. F. Hasan, A. T. Rafiqul, Determining Temperature and Time Dependent Poisson's Ratio of Asphalt Concrete using Indirect Tension Test, *Fuel* **2015**, *146*, 119 – 124.

[8] D. L. Chen, T. C. Chiu, T. C. Chen, Using DMA to Simultaneously Acquire Young's Relaxation Modulus and Time-Dependent Poisson's Ratio of a Viscoelastic Material, *Procedia Eng.* **2014**, *79*, 153 – 159.

[9] L. Dong, R. S. Lakes, Frequency Dependence of Poisson's Ratio of Viscoelastic Elastomer Foam. *Cellular Polym.* **2011**, *30*, 277 – 285.

[10] B. Pan, J. Y. Yuan, L. P. Yu, Determination of Viscoelastic Poisson's Ratio of Solid Propellants Using an Accuracy-Enhanced 2D Digital Image Correlation Technique, *Propellants Explos. Pyrotech.* **2015**, DOI: 10.1002/prep.201500042.

[11] N. W. Tschoegl, W. G. Knauss, I. Emri, Poisson's Ratio in Viscoelasticity: A Critical Review, *Mech. Time-Dependent Mater.* **2002**, *6*, 3–51.

[12] J. J. Zhang, H. D. Sun, The Effect of Poisson Rate on Mechanics Properties of Solid Propellant, *Mech. Management Develop.* **2009**, *24*, 42 – 44.

[13] H. T. Chu, J. H. Chou, Poisson Ratio Effect on Stress Behavior of Propellant Grains under Ignition Loading, *J. Propul. Power* **2011**, *27*, 662 – 667.

[14] QJ 3228–2005, *Test Method of Poisson's Ratio of Composite Solid Propellants*, China Academy of Aerospace Standardization and Product Assurance, Beijing, China, **2006**.

[15] GJB 770B-2005, *Test Method of Propellants*, Commission on Science, Technology and Industry for National Defense, Beijing, China, **2006**.

[16] S. J. Zhi, B. Sun, J. W. Zhang, Storage Life Prediction for Solid Rocket Motor Grain in Consideration of Poisson's Ratio, *J. Solid Rocket Technol.* **2011**, *34*, 593 – 597.

[17] H. P. Kugler, R. G. Stacer, C. Steimle, Direct Measurement of Poisson's Ratio in Elastomers, *Rubber Chem. Technol.* **1990**, *63*, 473 – 487.

[18] T. L. Smith, Volume Changes and Dewetting in Glass Bead-Polyvinyl Chloride Elastometric Composites under Large Deformations, *Trans. Soc. Rheology* **1959**, *3*, 113 – 136.

[19] W. G. Knauss, The Investigation of the Mechanical Properties of Thermoviscoelastic Materials, *7th International Congress on Experimental Mechanics*, Las Veags, NV, USA, June 8–11, p. 92.

[20] W. H. Peters, W. F. Ranson, Digital Imaging Techniques in Experimental Stress Analysis, *Optical Eng.* **1982**, *21*, 427 – 431.

[21] I. Yamaguchi, Speckle Displacement and Decorrelation in the Diffraction and Image Fields for Small Object Deformation, *Optica Acta* **1981**, *28*, 1359 – 1376.

[22] H. A. Bruck, S. R. McNeil, M. A. Sutton, Digital Image Correlation using Newton-Raphson Method of Partial Differential Correction, *Experim. Mech.* **1989**, *29*, 261 – 267.

[23] H. Jin, H. A. Bruck, Theoretical Development for Pointwise Digital Image Correlation, *Optical Eng.* **2005**, *44*, 067003 – 067014.

[24] H. Jin, H. A. Bruck, Pointwise Digital Image Correlation using Genetic Algorithms, *Experim. Tech.* **2005**, *29*, 36 – 39.

[25] M. L. Williams, R. F. Landel, J. D. Ferry, The Temperature Dependence of Relaxation Mechanisms in a Morphous Polymers and other Glass Forming Liquids, *J. Am. Chem. Soc.* **1955**, *77*, 3701 – 3707.

Received: November 17, 2015
Revised: February 4, 2015
Published online: ■■ ■■, 0000

DOI: 10.1002/prep.201500313

FULL PAPERS

*H. R. Cui, G. J. Tang, Z. B. Shen**

■■–■■

Study on the Viscoelastic Poisson‘s Ratio of Solid Propellants Using Digital Image Correlation Method

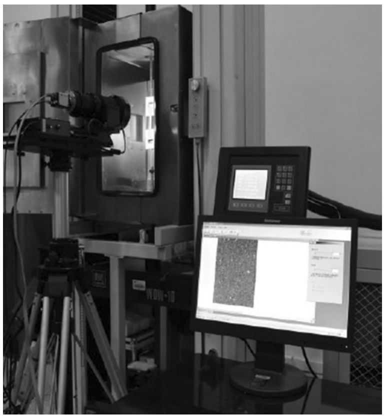

DOI: 10.1002/prep.201500313